ORIGINAL PAPER

THE INFLUENCE OF PRECURSORS ON THE MORPHO-STRUCTURE OF ZINC OXIDE

ECATERINA MAGDALENA MODAN[1], ADRIANA- GABRIELA SCHIOPU[2]*, CATALIN MARIAN DUCU [1,2], SORIN GEORGIAN MOGA[1], DENIS AURELIAN NEGREA[1], MIHAI OPROESCU[3], VASILE GABRIEL IANA[3], ADRIANA MIRUNA IOTA[4,5], OMAR AHMED[5]

Manuscript received: 16.02.2024; Accepted paper: 27.05.2024; Published online: 30.06.2024.

Abstract. *This paper presents the influence of different precursors on the morphostructure of zinc oxide nanoparticles used for the impregnation of polystyrene (PES) filters. Zinc oxide nanoparticles were synthesized by a microwave and ultrasound-assisted hydrolytic method using different precursors ($Zn(NO_3)_2$-$6H_2O$; $ZnSO_4$-$7H_2O$; and $Zn(CH_3COO)_2$-$2H_2O$) and sodium hydroxide as a nucleophilic agent. The resulting powders were calcined at 550 °C for 2 hours. Using the Williamson-Hall method for XRD analysis, the crystalline structure of the zinc oxide nanoparticles was determined, with average sizes of 40 nm (ZnO_AZ_US_MAE), 35.6 nm (ZnO_SU_US_MAE) and 36.4 nm (ZnO_AC_US_MAE). Morphological analysis by SEM revealed different shapes (polyhedral and irregular plates) with sizes ranging from 47 nm to 127 nm for the powder obtained from the zinc nitrate precursor, 43 nm to 63 nm for the powder prepared from the zinc sulfate precursor, and sizes ranging from 42 nm to 89 nm for the zinc acetate precursor. ATR FTIR spectroscopy was used to confirm the presence of Zn-O bonds. In addition, BET analysis showed that among the three Ipowders synthesized using different precursors, ZnO_SU_US_MAE had the highest surface area with a value of 16.4381 ± 0.0146 m²/g and an average particle size of 63.4671 nm, which was confirmed by SEM analysis.*

Keywords: *elaborate; ZnO nanoparticles; characterization of powders; impregnation of filters.*

[1] National University of Science and Technology POLITEHNICA Bucharest - Pitesti University Centre, Regional Center of Research & Development for Materials, Processes and Innovative Products Dedicated to the Automotive Industry (CRCD-AUTO), 110040 Pitesti, Romania. E-mail: ecaterina.modan@upb.ro; sorin.moga@upb.ro; denis.negrea@upb.ro; catalin.ducu@upb.ro.
[2] National University of Science and Technology POLITEHNICA Bucharest - Pitesti University Centre, Faculty of Mechanics and Technology, 110040 Pitesti, Romania.
[3] National University of Science and Technology POLITEHNICA Bucharest - Pitesti University Centre, Faculty of Electronics, Communication and Computers, 110040 Pitesti, Romania. E-mail : mihai.oproescu@upb.ro; vasile_gabriel.iana@upb.ro.
[4] National R&D Institute for Non-Ferrous and Rare Metals IMNR, 077145 Pantelimon, Romania. E-mail: iota.miruna@imnr.ro.
[5] National University of Science and Technology POLITEHNICA Bucharest, Science and Materials Engineering Doctoral School, Bucharest, Romania. E-mail: omaralssadi@yahoo.com.
* *Corresponding author:* gabriela.schiopu@upb.ro.

https://doi.org/10.46939/J.Sci.Arts-24.2-b01

1. INTRODUCTION

Zinc oxide (ZnO) is a wide-band-gap semiconductor material with a wide range of intriguing properties. ZnO crystallizes in the hexagonal wurtzite structure, characterized by a tetrahedral arrangement of oxygen atoms surrounding each zinc atom. ZnO boasts a large band gap of approximately 3.3 eV at room temperature [1-3]. This wide band gap translates to high transparency in the visible region, excellent electrical insulating properties in its pristine state, and high exciton binding energy (energy required to separate an electron-hole pair). ZnO can be doped with elements like Ga or In to become n-type semiconductors, finding use in electronics and optoelectronics [4, 5]. Due to its high transparency and tunable conductivity, ZnO is a promising candidate for transparent conducting oxide (TCO) electrodes in solar cells and touchscreens. ZnO's wide band gap makes it a good absorber of UV light, enabling its use in UV photodetectors for applications like flame sensors and environmental monitoring [6].

Synthesizing ZnO in various nanostructures such as nanorods, nanowires, and thin films has opened doors to novel applications [7-9]. These nanostructures exhibit enhanced properties compared to bulk ZnO due to increased surface area and quantum confinement effects. Integrating ZnO with polymers, ceramics, or other materials creates composites with synergistic properties. ZnO composites are being explored for applications in solar cells, light-emitting diodes (LEDs), and transparent conductors [10].

The precipitation method is a well-established and attractive route for synthesizing zinc oxide (ZnO) nanoparticles due to its simplicity, cost-effectiveness, and scalability. By adjusting reaction conditions, the size, morphology (spherical, rod-shaped, etc.), and crystallinity of the ZnO nanoparticles can be controlled to some extent [10-12]. The high surface area of nanoparticles can lead to aggregation, requiring additional processing steps like sonication or dispersing agents to achieve a uniform suspension.

Currently, various approaches exist to produce zinc oxide nanoparticles through both physical and chemical means. Each approach carries its own set of benefits and drawbacks, with primary concerns revolving around expenses, dimensions, and particle size uniformity [13]. Microwave irradiation can accelerate the reaction, potentially leading to faster synthesis and improved particle properties [14-17].

Therefore, the influence of different precursors on the morphostructure of zinc oxide (ZnO) nanoparticles used to impregnate polystyrene (PES) filters was investigated in this work. Three precursors ($Zn(NO_3)_2 \cdot 6H_2O$, $ZnSO_4 \cdot 7H_2O$, $Zn(CH_3COO)_2 \cdot 2H_2O$) and sodium hydroxide (NaOH) were used for the preparation of zinc oxide nanoparticles by hydrolytic synthesis assisted by microwaves and ultrasound. The developed powders were analyzed by morpho-structural characterization techniques using XRD, SEM-EDS, BET, and FTIR.

2. MATERIALS AND METHODS

2.1. MATERIALS

Zinc salt precursors of analytical purity $Zn(NO_3)_2 \cdot 6H_2O$, $ZnSO_4 \cdot 7H_2O$, $Zn(CH_3COO)_2 \cdot 2H_2O$ were purchased from Sigma Aldrich. Deionized water was used as the solvent for the synthesis and sodium hydroxide as the nucleophilic agent. PEG 4000 (Polyethylene Glycol) was employed to maintain stability.

Polyester filters, type G3, conform with SR EN 16890-1:2017 were procured from Pressing Vent.

2.2. ELABORATION OF ZINC OXIDE BY ASSISTED HYDROLYSIS OF ULTRASOUND AND MICROWAVE

ZnO powders were prepared by hydrolytic synthesis assisted by ultrasound and microwave using three zinc salt precursors, namely zinc nitrate, zinc sulfate, and zinc acetate, keeping the precursor/NaOH molar ratio at 0.5:1.

A volume of 50 ml of Zn $(NO_3)_2 \cdot 6H_2O$, 0.5 M was used during the synthesis process. This was achieved by dissolving 7.436 g Zn $(NO_3)_2 \cdot 6H_2O$ in 50 mL deionized water under magnetic stirring at room temperature to form a 0.5 M zinc nitrate solution. 50 L of 1M NaOH was added to the solution until a basic pH range was reached. To maintain the stability of the resulting precipitate, 0.1 g of PEG 4000 (polyethylene glycol) was added. The solution was then stirred in an ultrasonic bath for 10 minutes, followed by exposure to a microwave oven at 850 W for 5 minutes at a temperature of 65°C. After a short period at room temperature, the solution was filtered through filter paper and rinsed with deionized water and ethyl alcohol. The resulting precipitate was calcined at 550°C for 2 hours. The resulting powder was ground and designated ZnO_AZ_US_MAE.

Similarly, ZnO was prepared using zinc sulfate and zinc acetate precursors. The powder codes were ZnO_SU_US_MAE and ZnO_AC_US_MAE.

The following equipment was used for the ZnO preparation synthesis: a hydrolysis vessel, a magnetic stirrer equipped with a temperature sensor, a Thermo Scientific Eutech 5+ pH meter, a CD-4800 model ultrasonic bath with a frequency of 42 Hz, a Samsung microwave oven with a power range of 100-1500 W, and a Nabartherm heat treatment oven.

The specific experimental conditions for the hydrolytic synthesis facilitated by the ultrasonic and microwave methods are presented in Table 1.

Table 1. Conditions for ultrasound-assisted hydrolytic synthesis and microwaves.

Name samples	Precursor concentration	Nucleophilic agent	Frequency Time	Power Time	Temperature Calcining time
ZnO_AZ_US_MAE	0.5 M Zn $(NO_3)_2 \cdot 6H_2O$	1M NaOH	45 Hz 10 min	850 W 5 min	550˚C 2h
ZnO_SU_US_MAE	0.5 M $ZnSO_4 \cdot 7H_2O$				
ZnO_AC_US_MAE	0.5 M $Zn(CH_3COO)_2 \cdot 2H_2O$				

The equations of possible chemical reactions to create ZnO nanoparticles from precursors (e.g. zinc nitrate) in solution are shown below.

$$Zn(II)_{(aq)} + NaOH_{(aq)} \rightarrow Zn^{2+} + 2NO^{3-} + OH^-$$

$$Zn^{2+} + 2OH^- \rightarrow Zn(OH)_{2(aq)}$$

$$Zn(OH)_{2(aq)} \rightarrow ZnO_{(s)} + H_2O$$

2.3. MORPHO-STRUCTURAL CHARACTERIZATION TECHNIQUES

After the preparation of the zinc oxide powders, the microstructure of the powders was analyzed by X-ray diffraction using the Rigaku Ultima IV diffractometer with the CuKα

radiation source (λ=0.54(nm)). The diffractograms were taken in the 2θ range from 20° to 100°. The morphology and size of the zinc oxide powders were studied using the Hitachi SU 5000 scanning electron microscope.

For the molecular vibrational study, a Tensor 27 spectrometer (Bruker) was also used to obtain ATR (Attenuated Total Reflectance) - Fourier Transform Infrared (FTIR) spectra in the range 350-4000 cm^{-1} with a resolution of 4 cm^{-1}.

The powders were analyzed in a nitrogen atmosphere (absorption-desorption isotherms at 77 K). The moisture content of the samples was removed by degassing/drying at 300°C for approximately three hours before analysis. The BET surface area differs from sample to sample, as does the pore volume.

2.4. IMPREGNATION OF FILTERS WITH ZnO POWDERS PRODUCED BY ULTRASOUND AND MICROWAVE-ASSISTED HYDROLYTIC SYNTHESIS

Six pieces of PES filter material with an area of 5 cm^2 were cut. These were washed with deionized water and ethyl alcohol for decontamination. Afterward, 50 mg of ZnO obtained from the three precursors ($Zn(NO_3)_2 \cdot 6H_2O$, $ZnSO_4 \cdot H_2O$, $Zn(CH_3COO)_2 \cdot 2H_2O$) were weighed and dispersed in 50 ml of Tween solution at 7% concentration under magnetic stirring at 630 rpm for 20 min. To maintain the stability of the solutions obtained, 0.1 g of PEG 4000 (polyethylene glycol) was added to each solution and homogenized under ultrasound for 10 min.

One filter was immersed in the Berzelius beaker containing the solution with the sample code ZnO_AZ_US_MAE and afterward, placed in the ultrasonic bath for 10 minutes (sample code is PES-ZnO-AZ-US). The second filter was immersed in the same solution, which was magnetically stirred at 630 rpm for 20 minutes. The temperature of the solution in the beaker was 56˚C. The sample code is PES-ZnO-AZ-T. The two filters were placed in an oven for drying at150˚C for 15 minutes for the US-impregnated filter and 20 minutes for the temperature and shake-impregnated filter. The same procedure was followed for the other filters. The codes associated with the impregnated filters are PES_ZnO_SU_US, PES_ZnO_SU_T, PES_ZnO_AC_US and PES_ZnO_AC_T ZnO.

The impregnation process of ZnO filters developed by ultrasound and microwave-assisted hydrolytic synthesis is shown in Fig. 1.

Figure 1. Flux diagram of ZnO impregnated filters.

3. RESULTS AND DISCUSSION

3.1. X-RAY DIFFRACTION CHARACTERIZATION OF ZnO POWDERS

The structural properties of zinc oxide were determined by X-ray diffraction. The XRD pattern of ZnO nanoparticles is shown in Fig. 2.

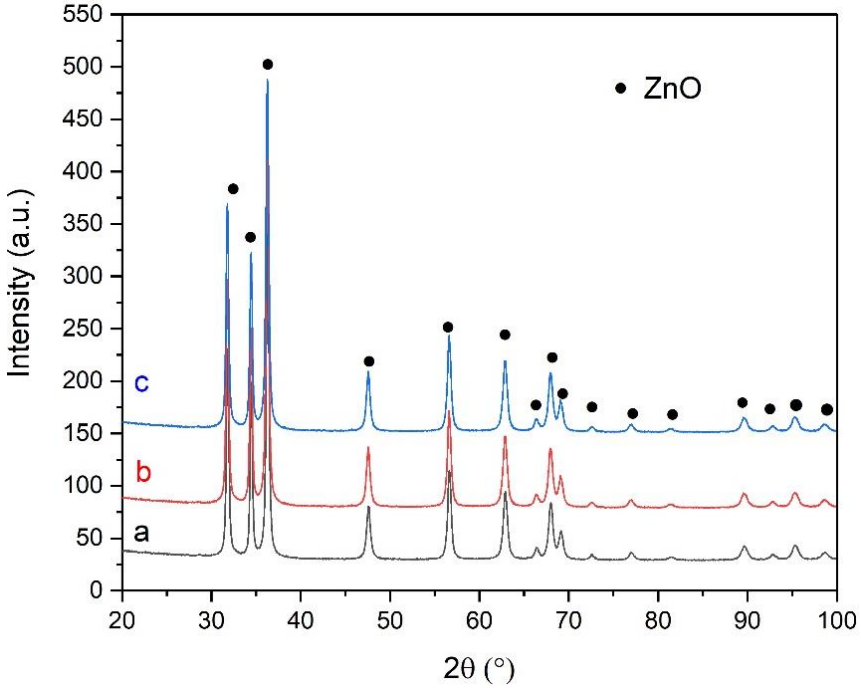

Figure 2. XRD patterns of XRD patterns of zinc oxide powders from different precursors: a) ZnO_AZ_US_MAE; b) ZnO_SU_US_MAE; c) ZnO_AC_US_MAE.

The peaks obtained correspond to the pure hexagonal wurtzite phase of ZnO. The superposition of the spectra shows the absence of other phases or impurities.

Table 2 shows the average crystallite size calculated by the Williamson-Hall method and the lattice parameters calculated by the WPPF method.

Table 2. Average crystallite size and lattice parameters.

Code samples	D (Å)	a (Å)	c (Å)
ZnO_AZ_US_MAE	400	3.2527	5.2114
ZnO_AC_US_MAE	364	3.2522	5.2109
ZnO_SU_US_MAE	356	3.2525	5.2099

The lattice parameter values are smaller compared to those found in scientific publications.

3.2. COMPOSITIONAL CHARACTERIZATION

The infrared spectrum recorded by the ATR-FTIR technique represents the "fingerprint" of each sample, obtained from the 3 precursors.

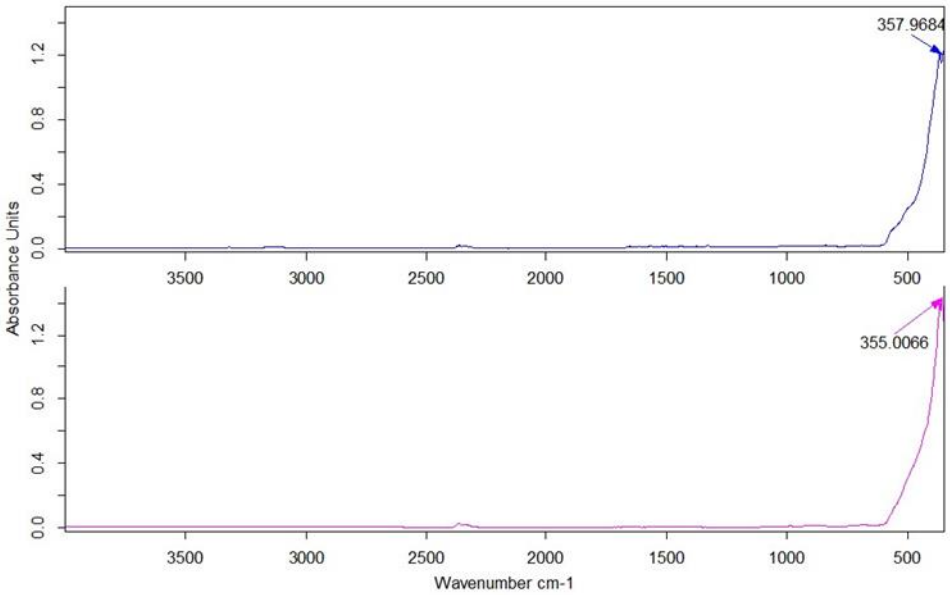

Figure 3. ATR-FTIR spectra of ZnO from nitrate (blue) and ZnO standard (magenta).

Analysis of the ATR-FTIR spectra in Fig. 3, showing the spectrum of standard commercial ZnO, compared to ZnO developed from nitrate precursor, reveals the existence of a wavelength of maximum absorbance corresponding to the Zn-O bond vibration. The signal attributed to 357 cm^{-1} confirms the achievement of ZnO by microwave-assisted hydrolytic synthesis.

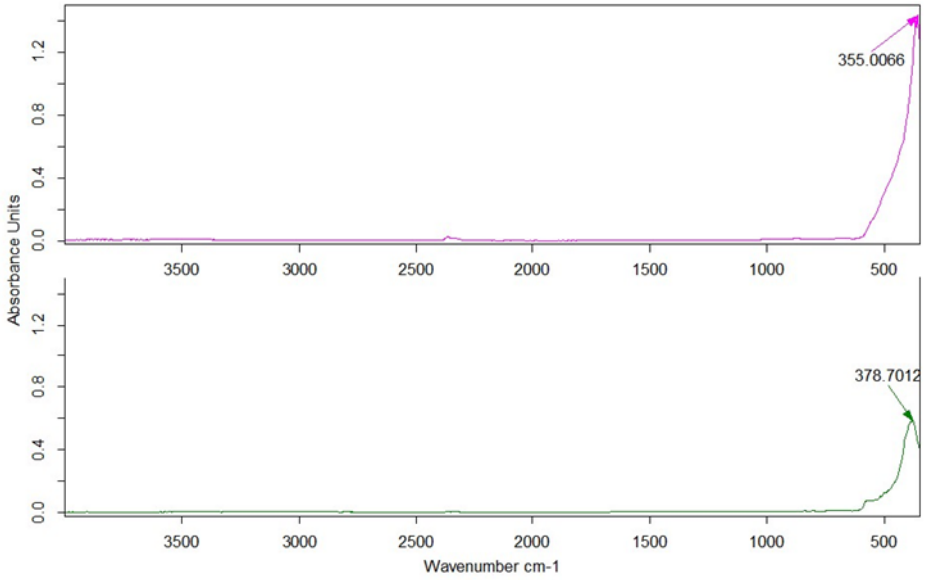

Figure 4. ATR-FTIR spectra of ZnO from sulfate (green) and ZnO standard (magenta).

Analysis of the ATR-FTIR spectra in Fig. 4, showing the commercial ZnO spectrum, compared to ZnO developed from sulfate precursor, reveals the existence of a wavelength of maximum absorbance corresponding to the Zn-O bond vibration. In the case of microwave-assisted hydrolytic synthesis from the sulfate precursor, a Zn-O vibration shift at approximately 378 cm^{-1} was revealed.

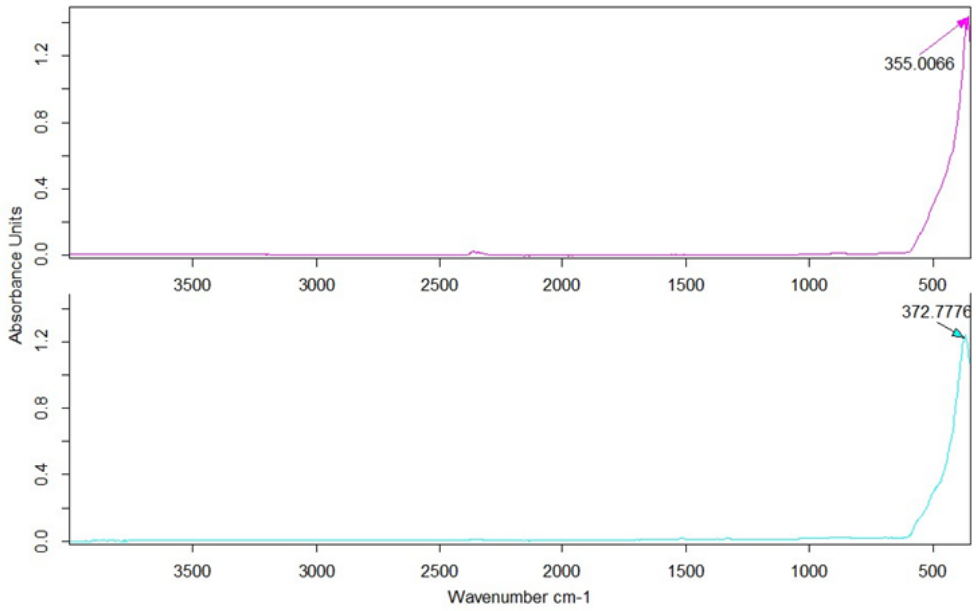

Figure 5. ATR-FTIR spectra of ZnO from acetate (turquoise) and ZnO standard (magenta).

Analysis of the ATR-FTIR spectra in Fig. 5, showing the spectrum of standard commercial ZnO, compared to ZnO developed from precursor acetate, reveals the existence of a wavelength of maximum absorbance corresponding to the Zn-O bond vibration. In the case of microwave-assisted hydrolytic synthesis from the precursor acetate, a Zn-O vibration turns of approximately 372 cm^{-1}. Since the ZnO spectrum, elaborated by hydrolytic synthesis, has no other peaks, it can be stated that it is pure.

3.3. MORPHOLOGICAL CHARACTERISATION OF ZnO POWDERS

For the morphological analysis of zinc oxide obtained by microwave and ultrasound-assisted hydrolytic synthesis, an electron microscope, Hitachi SU5000, was used. Fig. 6 shows the SEM micrographs for zinc oxide from different precursors (zinc nitrate, sulfate, and acetate).

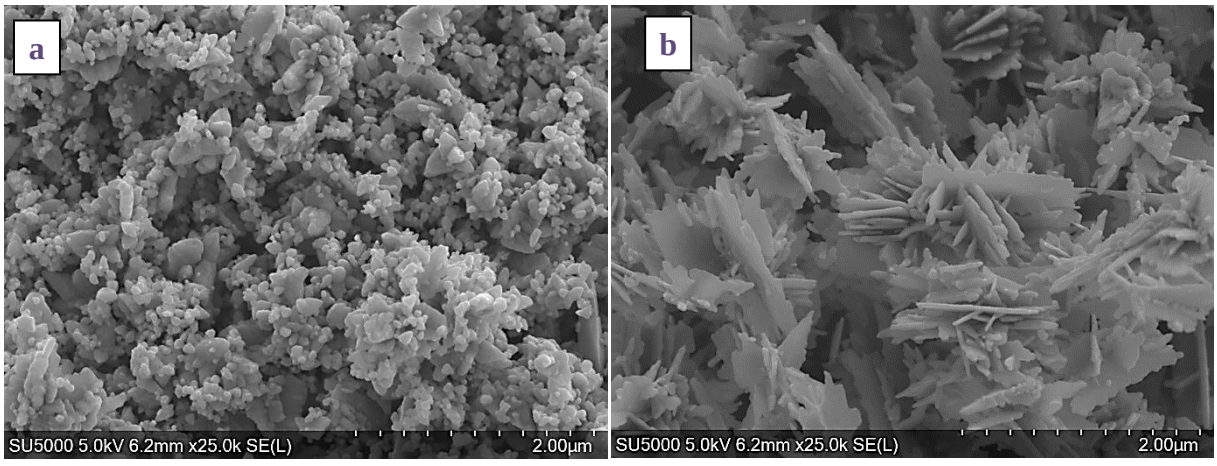

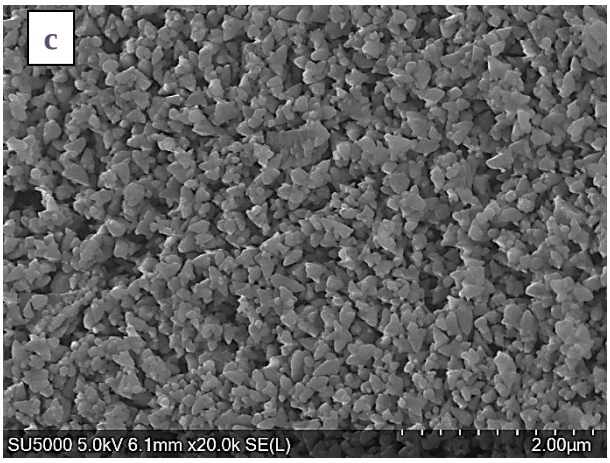

Figure 6. SEM micrograph of ZnO nanoparticles elaborated from different precursors: a) ZnO_AZ_US_MAE; b) ZnO_SU_US_MAE; c) ZnO_AC_US_MAE.

Irregular polyhedral shapes were identified for the zinc oxide powder obtained from the zinc nitrate precursor, with sizes ranging from 47 nm to 127 nm. In the case of the zinc oxide powder obtained from the zinc sulfate precursor, plates with thicknesses between 43 nm and 63 nm were observed. In the case of zinc oxide powder from zinc acetate precursor, irregular polyhedra with sizes ranging from 42 nm to 89 nm were also observed.

3.4. BET SURFACE AREA ANALYSIS

BET surface area analysis is the most common method for measuring the surface area of ZnO nanoparticles. This method involves measuring the amount of gas that can be adsorbed onto the surface of the nanoparticles. The surface area is then calculated using the BET equation. The experimental values for BET surface, total pore volume, and maximum pore volume are presented in Table 3.

Table 3. BET results of ZnO NPs elaborated by microwave-assisted hydrolytic synthesis with different precursors.

Nr.crt.	Code samples	Surface area [m^2/g]	Total pore volume [cm^3/g]	Nanoparticle size average (BET) [nm]	Max. pore volume [cm^3/g]
1.	ZnO/AZ_US_MAE	8.1573 ± 0.0083	0.015097	131.1124	0.003359
2.	ZnO/AC_US_MAE	12.0835 ± 0.0283	0.020553	88.5109	0.004891
3.	ZnO/SU_US_MAE	16.4381 ± 0.0146	0.032585	63.4671	0.006864

The surface area of ZnO nanoparticles is an important property that affects their reactivity and performance in a variety of applications. ZnO nanoparticles with a high surface area can present a large number of active sites, and this can lead to increased catalytic activity, photocatalytic activity, and gas adsorption capacity.

3.5. CHARACTERISATION OF IMPREGNATED FILTERS BY SEM-EDS

Fig.7 shows an image (SEM) of the PES filter impregnated with zinc oxide nanoparticles. Supplementary Figs. 7b and 7c show the corresponding energy dispersive X-ray spectroscopy (EDS) results. The elemental mapping shows the binding of Zn and O elements to the PES fibers, thus validating the impregnation process.

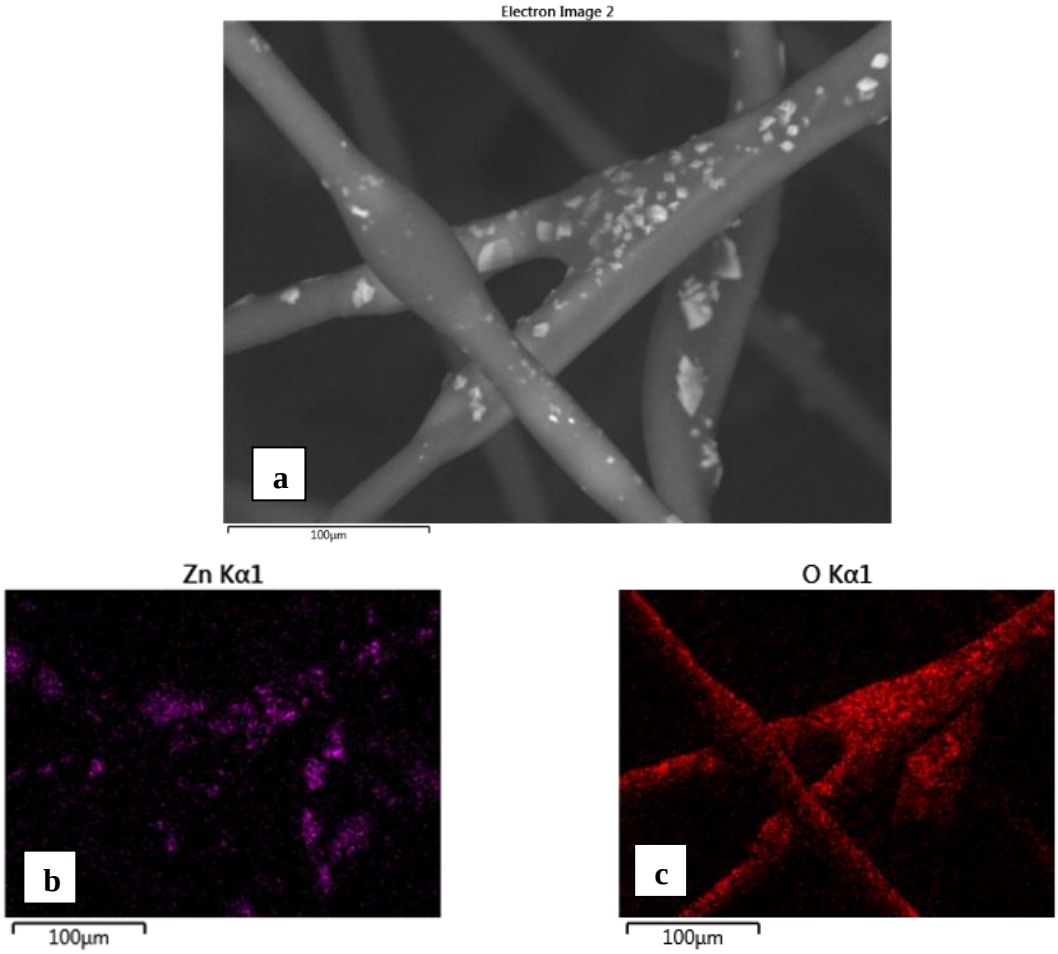

Figure 7. a) Representative SEM micrographs of PES filter impregnated with ZnO powder; b) and c) EDS mapping and elemental analysis including Zn (b) and O (c).

4. CONCLUSIONS

This paper investigates the effect of different precursors on the morphostructure of zinc oxide (ZnO) nanoparticles used to impregnate polystyrene filters. Zinc oxide nanoparticles were successfully developed by microwave and ultrasound-assisted hydrolytic synthesis. Three precursors, namely zinc nitrate, zinc sulfate, and zinc acetate, were used in the synthesis process, each resulting in different morphological characteristics.

Crystalline structure: XRD analysis confirmed the formation of ZnO nanoparticles in the hexagonal wurtzite phase, with no other impurities. The crystallite size ranged from 35.6 nm to 40 nm, with lattice parameters consistent with the hexagonal structure of wurtzite. SEM revealed variations in particle shape, and size depending on the precursor used. Irregular polyhedral and plates ranging in size from 42 nm to 127 nm were observed. The morphology

was different for each precursor: polyhedral and irregular plates for zinc nitrate, plates for zinc sulfate, and irregular polyhedral for zinc acetate. Analysis of ATR-FTIR spectra confirmed the presence of Zn-O bonds in all samples, indicating the successful synthesis of ZnO nanoparticles using the selected precursors. BET analysis showed the difference in surface area between the synthesized ZnO nanoparticles. ZnO__US_MAE exhibited the highest surface area of 16.4381 ± 0.0146 m^2/g, indicating its potential for reactivity and established performance in various applications.

The developed ZnO nanoparticles were successfully impregnated into P-filters as confirmed by SEM and energy dispersive X-ray spectroscopy (EDS). Elemental mapping showed the presence of zinc and oxygen elements on the PES fibers, validating the impregnation process.

The surface area of ZnO nanoparticles is a crucial property that governs their behavior in numerous applications. By controlling the synthesis method, particle size, and morphology, ZnO nanoparticles with high surface areas can be synthesized, leading to enhanced reactivity and improved performance in various applications.

REFERENCES

[1] Muhammad, J., Sonam Ghulam, H., Nasir, A., Waheed Qamar, K., *Results in Chemistry,* **5**, 100961, 2023.
[2] Samir, M., Musleh, H.S., Shaat, N., Assad, J., Al Dahoudi, N., *Materials Today Communications*, **35**, 105688, 2023.
[3] Khagendra, P., Dhurba, S., Manoj, K., Jamarkattel, C.P., *Nanomaterials*, **13**, 1795, 2023.
[4] Yufeng, Z., Wenxiong, Z., Qiuchen, W., Xinlu, L., Ziyao, Z., Yuhang, L., Kai, H., Xiangxin, L., *RSC Advances* **13**, 9503, 2023.
[5] Liu, G., Rahman, E., Ban, D., *Journal of Applied Physics*, **118**, 094307, 2017.
[6] Yu, Z., Xia, Y., Du, D., Ouyang, J., *ACS Applied Materials & Interfaces*, **8**, 11629, 2016.
[7] Schlur, L., Calado, J.R., Spitzer, D., *Royal Society Open Science*, ***5***, 180510, 2018.
[8] Huang, M.H., Wu, Y., Feick, H., Tran, N., Weber, E., Yang, P., *Advanced Materials*, **13**, 113, 2001.
[9] Podia, M., Tripathi, A.K., *Journal of Luminescence*, **252**, 119331, 2022.
[10] Yue, S., Wei, Z., Qun, L., Huijie, L., Xiaolei, W., *Advanced Sensor and Energy Materials*, **2**, 100069, 2023.
[11] Nida, K., Sermin, O., Tülay, Y., Ayça, K., *Science of Sintering*, **54**, 73, 2022.
[12] Seyed Sharifodin H., Ali Mohammad S., Mohammad Shafiey D., *Physics of Fluids*, **34**(9), 092008, 2022.
[13] Malinovschi, V., Andrei, V., Coaca, E., Mihailescu, C.N., Lungu, C.P., Radulescu, C., Dulama, I.D., *Surface and Coatings Technology*, **375**, 621, 2019.
[14] Hasanpoor, M., Aliofkhazraei, M., Delavari, H., *Procedia Materials Science***, 11**, 320, 2015.
[15] Modan, E.M., Ducu, Topala, C.M., C.M., Moga, S.G., Negrea, D.A., Plaiasu, A.G., *Journal of Science and Arts*, **4**, 1081, 2021.
[16] Andrei, V.A., Radulescu, C., Malinovschi, V., Marin, A., Coaca, E., Mihalache, M., Mihailescu, C.N., Dulama, I.D., Teodorescu, S., Bucurica, I.A., *Coatings*, **10**(4), 318, 2020.
[17] Bintintan, A., Gligor, M., Radulescu, C., Dulama, I.D., Olteanu, R.L., Teodorescu, S., Stirbescu, R.M., Bucurica, I.A., *Analytical Letters*, **52**(15), 2348, 2019.